Research in Astronomy and Astrophysics, 23:065019 (8pp), 2023 June https://doi.org/10.1088/1674-4527/accbae

The Bar-Bulge Relation in Non-dwarf SB0 Galaxies in the Central Region of Coma Cluster

Nagamani Poloji[1], Priya Hasan[2], and S. N. Hasan[3]
[1] Department of Astronomy, Osmania University, Hyderabad, India; priya.hasan@gmail.com
[2] Department of Physics, Maulana Azad National Urdu University, Hyderabad, India
[3] Department of Mathematics, Maulana Azad National Urdu University, Hyderabad, India
Received 2022 November 26; revised 2023 February 26; accepted 2023 March 10; published 2023 May 30

Abstract

In this paper we explore the formation of bars and present the bulge and bar properties and their correlations for a sample of lenticular barred (SB0) and lenticular unbarred (S0) galaxies in the central region of the Coma Cluster using HST/ACS data. In our sample, we identified bar features using the luminosity profile decomposition software GALFIT. We classified the bulges based on Sérsic index and Kormendy relation. We found that the average mass of the bulge in SB0 galaxies is $1.48 \times 10^{10}\ M_\odot$ whereas the average mass of the bulge in S0 galaxies is $4.3 \times 10^{10}\ M_\odot$. We observe that SB0 galaxies show lower bulge concentration, low mass and also smaller B/T values compared to S0 galaxies. Using the Kormendy relation, we found that among the lenticular barred galaxies, 82% have classical bulges and 18% have pseudo bulges. These classical bulges have low masses compared to the classical bulges of unbarred galaxies. S0, galaxies with massive classical bulges do not host bars. We also found that for all SB0s the bulge effective radius is less than the bar effective radius. SB0 galaxies with classical bulges suggest that the bar may have formed by mergers.

Key words: galaxies: clusters: individual (Coma) – galaxies: bulges – galaxies: elliptical and lenticular – cD

1. Introduction

Bars are common features in spiral galaxies, thought to be formed by isolated secular processes (Cavanagh & Bekki 2020). Low luminosity lenticulars also exhibit bar features (Barway et al. 2011). Previous studies report that the fraction of barred galaxies decreases with redshift (Nair & Abraham 2010), but some observations show similar bar fractions for $z \sim 1$ (Elmegreen et al. 2004; Jogee et al. 2004; Marinova et al. 2007). The bar fraction does not appear to change from lower to higher density regions (Méndez-Abreu et al. 2010; Marinova et al. 2012; Lansbury et al. 2014). However, the bar fraction of galaxies varies with morphological type. It is observed that in the field, bars are often present in spiral galaxies, while in clusters, lenticulars often have bars (Hubble & Humason 1931; Fasano et al. 2000; Helsdon & Ponman 2003; Deng et al. 2009).

Bulge properties are related to bar formation and its strength (Skibba et al. 2012). Bulges are classified into classical and pseudo bulges, where classical bulges have a Sérsic index $n > 2$ and pseudo bulges have $n < 2$ (Fisher & Drory 2008). Classical bulges are a result of major mergers and/or multiple minor mergers (Hopkins et al. 2010; Kormendy 2013). Pseudo bulges are formed by secular evolution (Kormendy & Kennicutt 2004; Kormendy 2013). Poloji et al. (2022a) found that in the central region of Coma Cluster the $B/T \geqslant 0.3$ galaxies with classical bulges may have formed by mergers and $B/T \leqslant 0.3$ galaxies with pseudo bulges may have formed by a secular process.

N-body simulations show that massive bulges prevent the formation of bars in galaxies. Disks are heated due to the large mass in bulges and hence are unable to host bars (Athanassoula et al. 2005; Kataria & Das 2018).

Based on theoretical studies, bars can form in three scenarios: in isolation, tidal interactions and galaxy mergers (Cavanagh & Bekki 2020). In the isolated scenario, bars form in self-gravitating, rotating disks when most of the kinetic energy is in rotational motion, which happens in cold disks (Kalnajs 1972). In tidal interactions, the bar forms when low mass satellite galaxies interact with their host (Toomre & Toomre 1972; Athanassoula 1999). In galaxy mergers, mergers with minor satellites and larger galaxies can result in bar formation (Gerin et al. 1990; Mayer & Wadsley 2004; Peirani et al. 2009). However, often major mergers destroy the bar (Cavanagh & Bekki 2020). Bars in cluster environments have different characteristics compared to their isolated counterparts which is probably a result of frequent encounters (Elmegreen et al. 1990).

The Coma Cluster is a rich and dense cD cluster at a redshift of 0.023 which corresponds to an approximate distance of 100 Mpc (Carter et al. 2008). This is a suitable cluster to study bulge and bar properties of galaxies. In previous papers, Méndez-Abreu et al. (2010) studied bars in galaxies and found that the bar fraction does not vary significantly from the cluster center to outskirts. Marinova et al. (2012) concluded that the bar fraction among lenticulars is not enhanced in rich clusters compared to low density environments, i.e., is similar irrespective of environment. However, Lansbury et al. (2014) ascertained that there is an increase in the bar fraction toward the cluster core, at a low significance level. In general, bars have a weak correlation with distance from the cluster center.

In our papers (Poloji et al. 2022a, 2022b), we studied the structural properties and morphology of galaxies in the central region of the Coma Cluster brighter than 19.5^m in the $F814W$ band from the HST/ACS Coma Cluster Treasury Survey. In this paper, we aim to study the bulge and bar properties such as concentration, mass, B/T, etc. and their correlations for the sample of S0 and SB0 galaxies described in our above mentioned paper.

The paper is structured as follows: Section 1 of the paper gives a brief introduction and a description of the problem. Section 2 describes the data and sample selection. Section 3 addresses the bar identification and structural decomposition using GALFIT. Section 4 elucidates the bulge classification. Section 5 explains the role of bulges in the bar formation. Section 6 describes the interplay between bulge and bar in SB0 galaxies and Section 7 provides the discussions and conclusions of this paper.

2. Sample Selection

In this paper, we use publicly available data[4] from the HST/ACS Coma Cluster Treasury survey (Carter et al. 2008). This survey was 28% complete, because of the ACS failure. It has data in two filters, $F814W$ and $F475W$, with exposures of 1400 s and 2560 s, respectively. The observations cover 25 fields of which 19 are located within 0.5 Mpc of the center and the remaining 6 are located at the southwest extension of the cluster.

Cluster membership was determined using spectroscopic redshifts, the details of which are available in Poloji et al. (2022b). We only selected non-dwarfs in our sample as the bulge-disk-bar decomposition of GALFIT only worked well for these galaxies. This implies an absolute magnitude limit $F814W \leqslant -18.5^m$ (Marinova et al. 2012).

In our earlier paper Poloji et al. (2022a), we presented the results of visual classification for this sample of 219 galaxies in the central region of the Coma Cluster and selected our sample of S0 galaxies. Our final sample has 11 lenticular galaxies with bars (SB0) and 15 S0 galaxies without bars (S0). To calculate galaxy masses, we followed Weinzirl et al. (2014). Using $I = F814W - 0.38$, we converted AB magnitude to the Vega (Cousins-Johnson) system and, from the WFPC2 Photometry Cookbook, we calculated colors as

$$B - I = 1.287(F475W - F814W) + 0.538,$$

(Price et al. 2009). We calculated the mass–luminosity relationship M/L from Into & Portinari (2013).

$$I_{\rm lum} = 10^{(-0.4(I-35-4.08))},$$

$$M_* = I_{\rm lum} \times 10^{(0.641(B-I)-0.997)},$$

where I corresponds to the apparent MAG_AUTO SExtractor magnitude, 35 is the distance modulus to Coma and 4.08 is the solar absolute magnitude in I band. To calculate the mass of bulge, disk and bar we considered the color of the galaxy from the SExtractor catalog (Bertin & Arnouts 1996; Hammer et al. 2010).

3. Bar Identification and Structural Decomposition

To identify bars and their properties we used GALFIT (Peng et al. 2002). We preferred using GALFIT as this is a two-dimensional technique compared to the alternative IRAF ellipse method. The main benefit with two-dimensional profiles is the full use of spatial information and a better estimate of image blurring by the point-spread function (PSF). Also, Marinova et al. (2012) used the IRAF ellipse task as well as GALFIT visual method to identify the bar features in S0 galaxies and they found similar results using both methods. Also, GALFIT gives additional parameters for each component such as the Sérsic index, effective radius, etc., which have been used in our analysis. We do a three component decomposition: bulge, bar and disk. To fit the bulge and bar we relied on Sérsic profiles and for the disk we utilized exponential profiles (Freeman 1970). The Sérsic profile is described as

$$I(r) = I_e \exp(-b_n((r/r_e 1/n) - 1)),$$

where $I(r)$ is the intensity at distance r from the center, r_e is the effective radius within which half of the total light of the galaxy is contained, I_e is the intensity at r_e, n is the Sérsic index and the constant b_n defined in terms of n describes the shape of the light-profile. Generally, $b_n = 1.9992 * n - 0.3271$ (Capaccioli 1989).

The details of structural decomposition have been described in Poloji et al. (2022b). Sky background as well as the GALFIT input parameters, *viz.*, MAG_AUTO = F814W, FLUX_RADIUS[3] = r_e, ELLIPTICITY = b/a and THETA_IMAGE = position angle were taken from the SExtractor catalog (Hammer et al. 2010). We generated a PSF from TinyTim (Krist et al. 2011). We produced a mask for each galaxy to exclude neighboring sources using IRAF. Figure 1 features sample images of three galaxies where the leftmost is the science image, center is the model image and the rightmost is the residual image. A figure with the complete sample of SB0 galaxies can be provided on request.

We identified the bar and bulge component based on Sérsic index (n), where the lower n, higher effective radius and axis

[4] https://archive.stsci.edu/prepds/coma/datalist2.1.html

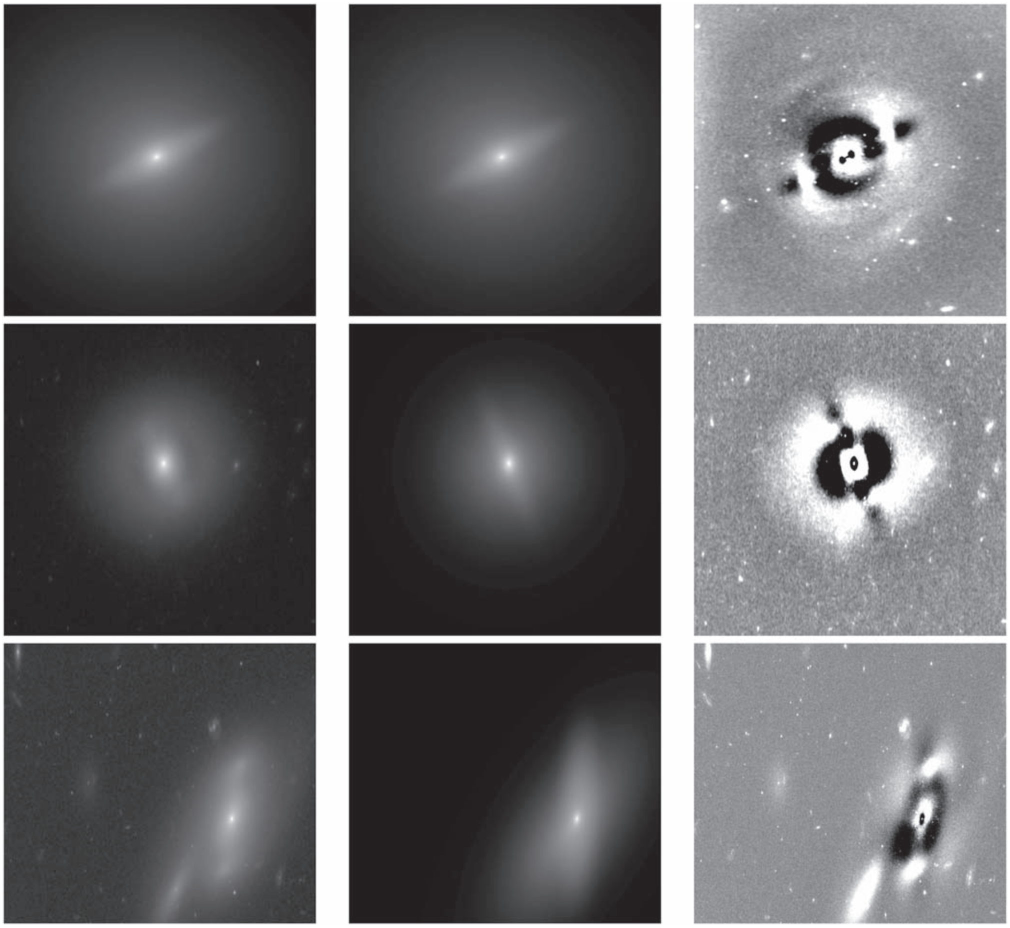

Figure 1. The figure displays sample results of bulge-disk-bar decomposition by GALFIT. The first column shows the science images, middle column depicts GALFIT model images and the third column displays residuals which are obtained by subtracting the model image from the science image. The galaxies are: COMAi13042.832p275746.95, COMAi13027.966p275721.56 and COMAi125956.697p275548.71.

ratio (b/a) belong to the bar of the galaxy. Tables 1 and 2 describe the output parameters and will be available on request.

Due to the small sample size, we tested our hypothesis to check if members have a significantly higher number of E/S0 galaxies than non-members. The Fisher exact test yielded $p = 0.037$. We did the chi^2 test and found the chi^2 statistic (=4.8799) for $p = 0.027171$. The result is significant using both the Fisher's and chi^2 tests, confirming our hypothesis and recognizing that this cluster has a majority of E and SOs. This signifies that there are sufficient data to conclude that the distributions differ (i.e., the cluster and the field) and hence our results apply to galaxies in a cluster.

4. Bulge Classification

To classify bulges, a key parameter is the Sérsic index (Sersic 1968) where classical bulges have a Sérsic index $n \geqslant 2$ and pseudo bulges have $n < 2$ (Fisher & Drory 2008; Gadotti 2008; Vaghmare et al. 2013). Often pseudo bulges are found in galaxies with features like bars, disks and spiral arms (Carollo et al. 1998; Fisher & Drory 2008). Galaxies with classical bulges generally lack such features.

Using the Sérsic index, we classified our sample and found that 64% have classical bulges and 36% pseudo bulges. The errors in the fit of Sérsic index (n) can be as large as 20% which corresponds to an error as large as 0.5 (Gadotti 2008; Vaghmare et al. 2013) and hence we complement our results with the Kormendy diagram (Kormendy 1977). Gadotti (2009), Vaghmare et al. (2013), and Poloji et al. (2022a) demonstrated that this is a more robust method to classify bulges. The Kormendy diagram is a plot of the logarithm of the effective radius r_e of the bulge and its average surface brightness within the effective radius as depicted in Figure 2. Generally, this plot shows a tight linear correlation for elliptical galaxies with a slope more than three (Kormendy 1977). Elliptical galaxies were used to fit a straight line as displayed in the figure. Galaxies with classical bulges lie within 3σ of the above fit

Table 1
Results of Bulge-disk-bar Decomposition for our Sample

Col	Parameter	Description
1	COMA_ID	Name of source
2	R.A. (J2000)	Right ascension
3	Decl. (J2000)	Declination
4	Bm	Bulge magnitude
5	$Bm_{\rm error}$	Error in bulge magnitude
6	$BSB\mu_e$	Bulge surface brightness
7	Br_e	Bulge effective radius in arcsec
8	Bn	Bulge Sérsic index
9	$Bn_{\rm error}$	Error in bulge Sérsic index
10	Bb/a	Bulge axis ratio
11	$Bb/a_{\rm error}$	Error in bulge axis ratio
12	BPA	Bulge position angle
13	$BPA_{\rm error}$	Error in bulge position angle
14	Dm	Disk magnitude
15	$Dm_{\rm error}$	Error in disk magnitude
16	$DSB\mu_e$	Disk surface brightness
17	Dr_s	Disk scale length in arcsec
18	Db/a	Disk axis ratio
19	$Db/a_{\rm error}$	Error in disk axis ratio
20	DPA	Disk position angle
20	$DPA_{\rm error}$	Error in disk position angle
21	z	Redshift
22	B/T	Bulge to total light ratio
23	Morphology	Based on visual inspection
24	$Barm$	Bar magnitude
25	$Barm_{\rm error}$	Error in bar magnitude
26	$Bar\mu_e$	Bar surface brightness
27	$Barr_e$	Bar effective radius in arcsec
28	$Barn$	Bar Sérsic index
29	$Barn_{\rm error}$	Error in bar Sérsic index
30	$Barb/a$	Bar axis ratio
31	$Barb/a_{\rm error}$	Error in bar axis ratio
32	$BarPA$	Bar position angle
33	$BarPA_{\rm error}$	Error in bar position angle

while galaxies with pseudo bulges lie outside the 3σ of the best fit line of ellipticals (Gadotti 2009). We have plotted the $\pm 3\sigma$ and also $\pm 4\sigma$ lines because three SB0 galaxies (blue filled squares: COMAi125710.760p272417.38, COMAi13038.761p 28052.34 and COMAi13042.832p275746.95) with Sérsic indices close to classical bulges 2.81, 1.88 and 3.21 lie slightly below the 3σ line, but within the 4σ lines (gray dotted lines) (Figure 2). Using this method, we found that our sample has 82% classical bulges and 18% pseudo bulges.

5. Role of Bulges in Bar Formation

Many studies suggest that the formation of bars depends on the mass of the bulge (Athanassoula et al. 2005; Kataria & Das 2018). Low mass, cold and rotationally supported disks in galaxies support bars. According to simulations done by Kataria & Das (2018), bulge mass and concentration play an important role in the formation of bars in disk galaxies. Bulge concentration is the ratio of bulge effective radius (r_e) to the disk scale length (r_s). In Figure 3 we plot the relation between bulge mass and bulge concentration of SB0 (blue filled squares) and S0 (red filled circles) galaxies. It is clear the SB0 galaxies have low bulge masses. The vertical dashed line is at $M_{\rm bulge} = 2.73 \times 10^{10}\ M_{\odot}$, where $\log M_{\rm bulge} = 10.4$ marks the upper limit for masses of the bulge of SB0 galaxies. We observe that SB0 galaxies show a lower bulge concentration and low mass compared to S0 galaxies. The horizontal dashed line separates the S0 and SB0 galaxies at -0.4 in the logarithmic scale of bulge concentration (except for two S0 galaxies). These two S0 galaxies have low bulge concentrations. Of these, one S0 galaxy (COMAi125931.453p28247.60) has a large error in disk scale length (r_s) and the other S0 galaxy (COMAi13016.534p275803.15) is an edge-on galaxy, which is probably an explanation of their location. Figure 3 shows a plot of logarithm of mass of the bulge and the logarithm of the ratio of bulge effective radius (r_e) and disk scale length (r_s). Here blue filled squares represent the SB0 galaxies and red filled circles are the S0 galaxies. The horizontal dashed line separates the S0 and SB0 galaxies at -0.4 for logarithm of bulge concentration except for two S0 galaxies. It is also clear the SB0 galaxies have low bulge masses. The vertical dashed line is at $M_{\rm bulge} = 2.73 \times 10^{10}\ M_{\odot}$, where $\log M_{\rm bulge} = 10.4$ marks the upper limit for masses of the bulge of SB0 galaxies.

In Figure 4 we plot the B/T distribution of S0 and SB0 galaxies and note that SB0 galaxies have a smaller B/T distribution (<0.42) compared to S0 galaxies, which implies smaller bulges. It thus appears that, to form bars, galaxies should preferably have lower bulge masses and fainter luminosities. We find that the average mass of bulges in SB0 galaxies is $1.48 \times 10^{10}\ M_{\odot}$ and the average mass of bulges in S0 galaxies is $4.3 \times 10^{10}\ M_{\odot}$.

6. The Interplay between Bulges and Bars in SB0 Galaxies

In Section 5 we have seen that the bar strongly depends on the properties of the bulge.

In our sample of SB0 galaxies, we found that 64% of the bulges which have bars have Sérsic index $n \geqslant 2$ and are classical bulges, possibly formed by mergers (Kormendy & Kennicutt 2004; Fisher & Drory 2008; Kormendy 2013).

It is also important to understand whether the bar formed before or after the mergers that led to classical bulges. Numerical simulations show that bars can be formed by galaxy merging (Peirani et al. 2009). Specifically for SB0 galaxies, bars can be formed by minor mergers (Cavanagh & Bekki 2020). Figure 5 depicts the mass distribution of classical bulges of S0 and SB0 galaxies, which again shows that bars form in low mass bulges.

Table 2
Results of Bulge-disk and Bar Decomposition

			Bulge properties										Disk properties									Bar properties									
COMA_ID	R.A.	Decl.	Bm	Bmerr	Bre	BSB	Bn	Bnerr	Bb/a	Bb/aerr	BPA	Bpaerr	Dm	Dmerr	Drs	DSB	Db/a	Db/aerr	DPA	DPAerr	B/T	Barm	Barmerr	BarSB	Barre	Barn	Barnerr	Barb/a	Barb/aerr	BarPA	BarpAerr
COMAi13018.772p275613.34	195.08	27.94	18.83	0.08	0.64	19.05	0.79	0.03	0.34	0.01	−77.04	0.54	16.5	0.0001	2.64	19.8	0.98	0.0008	−62.07	2.8	0.07	17.34	0.02	20.77	2.8	0.77	0.02	0.23	0.002	−78.38	0.12
COMAi125710.760p272417.38	194.29	27.4	16.51	0.01	0.71	16.95	2.81	0.03	0.93	0.001	−9.93	1.65	14.25	0.04	12.92	21.0	0.95	0.004	72.72	1.13	0.09	15.75	0.01	20.43	4.98	0.68	0.001	0.72	0.003	−3.34	0.1
COMAi125956.697p275548.71	194.99	27.93	17.4	0.01	0.55	17.31	2.04	0.03	0.77	0.001	−34.08	0.99	15.79	0.0001	4.03	20.01	0.47	0.001	−53.08	0.07	0.13	16.51	0.01	20.73	4.04	0.48	0.001	0.46	0.0007	−7.22	0.12
COMAi125946.782p275825.99	194.94	27.97	16.68	0.0002	0.46	16.2	1.42	0.01	0.78	0.002	−87.68	0.52	14.83	0.0001	3.4	18.68	0.72	0.002	84.25	0.04	0.13	16.69	0.0002	19.67	2.28	0.65	0.01	0.38	0.004	−37.34	0.1
COMAi13017.014p28350.07	195.07	28.06	16.15	0.04	0.4	15.33	2.64	0.07	0.82	0.001	−30.83	1.68	15.19	0.0002	2.76	20.39	0.6	0.001	−27.63	0.09	0.22	16.02	0.03	18.67	1.34	0.62	0.01	0.61	0.01	14.33	0.31
COMAi13038.761p28052.34	195.16	28.01	16.39	0.01	0.92	17.41	1.88	0.02	0.68	0.002	−20.67	0.09	16.71	0.01	2.42	19.82	0.6	0.0007	−59.92	9.0	0.3	15.89	0.02	20.54	4.9	0.63	0.02	0.44	0.002	−25.5	0.84
COMAi13042.832p275746.95	195.18	27.96	15.71	0.0003	1.47	17.75	3.21	0.01	0.76	0.002	−33.89	0.15	15.0	0.0001	5.56	19.92	0.82	0.0005	10.28	0.07	0.32	17.52	0.01	20.92	2.76	0.34	0.002	0.28	0.001	−55.89	0.05
COMAi13027.966p275721.56	195.12	27.96	16.28	0.0003	0.48	15.88	1.67	0.01	0.83	0.002	87.21	0.5	15.62	0.0003	2.75	19.01	0.62	0.001	−88.82	0.06	0.32	17.72	0.01	20.89	2.48	0.52	0.01	0.36	0.003	36.55	0.19
COMAi13042.766p275817.38	195.18	27.97	14.54	0.02	1.69	16.87	2.51	0.03	0.89	0.001	−35.1	0.24	13.79	0.0003	13.84	20.69	0.83	0.004	43.89	0.09	0.33	17.98	0.0001	21.33	2.7	0.15	0.002	0.26	0.002	−33.14	0.07
COMAi125930.824p275303.05	194.88	27.88	14.48	0.0002	0.95	15.57	2.05	0.001	0.82	0.002	18.43	0.16	14.32	0.0003	7.43	23.09	0.62	0.001	33.42	0.03	0.4	15.72	0.0001	22.67	3.2	0.36	0.002	0.54	0.002	65.41	0.08
COMAi13022.170p28249.30	195.09	28.05	15.26	0.0003	1.54	17.39	2.23	0.001	0.77	0.002	21.0	0.14	15.36	0.0021	7.81	21.01	0.72	0.0007	−63.46	0.09	0.42	16.03	0.0001	20.91	5.45	0.3	0.002	0.71	0.001	−42.47	0.11
COMAi13016.534p275803.15	195.07	27.97	15.79	0.0031	0.44	15.2	1.73	0.01	0.74	0.001	−65.26	0.31	14.81	0.0001	2.3	13.6	0.42	0.001	−67.75	0.03	0.29										
COMAi125928.721p28225.92	194.87	28.04	14.79	1.01	1.15	16.28	2.1	1.02	0.51	0.001	87.95	0.14	15.06	0.02	2.23	12.84	0.62	0.001	70.45	0.29	0.56										
COMAi13005.405p28128.14	195.02	28.02	15.77	0.01	2.19	18.67	2.93	0.01	0.74	0.001	64.22	0.24	15.93	0.01	2.91	12.72	0.37	0.001	53.54	0.06	0.54										
COMAi13018.093p275723.59	195.08	27.96	14.66	0.0002	2.33	17.69	4.0	0.001	0.75	0.002	47.4	0.18	15.42	0.0001	0.88	13.44	0.94	0.002	10.21	1.39	0.67										
COMAi125944.407p275444.84	194.94	27.91	14.32	0.0002	2.11	17.14	3.58	0.01	0.79	0.002	−76.43	0.19	13.8	0.0002	2.08	11.0	0.57	0.001	−81.47	0.08	0.38										
COMAi125931.453p28247.60	194.88	28.05	13.5	0.0004	2.1	16.3	2.44	0.01	0.45	0.002	18.43	0.04	12.58	0.1	19.96	7.33	0.61	0.0007	−70.27	0.17	0.3										
COMAi125911.543p28033.32	194.8	28.01	16.93	0.02	0.91	17.92	1.28	0.02	0.65	0.001	54.23	0.5	16.64	0.01	1.32	15.24	0.96	0.001	−69.05	4.2	0.43										
COMAi125944.208p275730.38	194.93	27.96	15.13	0.01	5.94	20.19	6.45	0.09	0.46	0.001	−83.8	0.09	15.79	0.0002	1.45	12.25	0.44	0.001	−86.46	0.1	0.65										
COMAi125938.321p275913.89	194.91	27.99	13.64	0.02	24.01	21.73	5.63	0.05	0.63	0.002	−55.29	0.05	12.83	0.29	31.57	4.44	0.62	0.04	28.4	1.31	0.32										
COMAi125940.270p275805.71	194.92	27.97	15.62	0.01	1.86	18.16	6.58	0.04	0.81	0.001	−52.69	0.37	16.17	0.0001	1.56	13.83	0.43	0.001	−50.71	0.06	0.62										
COMAi13039.767p275526.19	195.17	27.92	14.07	0.01	1.95	16.71	3.05	0.01	0.8	0.002	−66.33	0.06	14.55	0.01	2.67	11.56	0.96	0.001	−57.53	0.7	0.61										
COMAi125820.530p272545.99	194.59	27.43	17.53	0.02	1.07	18.87	0.9	0.01	0.47	0.001	60.55	0.22	16.73	0.01	1.87	14.78	0.48	0.0006	65.03	0.08	0.32										
COMAi13028.370p275820.64	195.12	27.97	14.8	0.0003	2.73	18.18	2.49	0.01	0.47	0.001	−4.22	0.06	15.6	0.01	3.57	11.93	0.96	0.0003	6.37	2.05	0.68										
COMAi125904.797p28301.16	194.77	28.05	16.41	0.02	1.88	18.97	2.37	0.02	0.58	0.001	30.01	0.32	16.71	0.02	2.19	13.98	0.43	0.001	8.92	0.2	0.57										
COMAi125704.337p273133.28	194.27	27.53	16.2	0.09	2.83	19.65	0.99	0.01	0.34	0.01	−80.53	0.13	16.73	0.15	1.91	13.71	0.49	0.01	−78.7	0.28	0.62										

Note. Table description can be seen in Table 1.

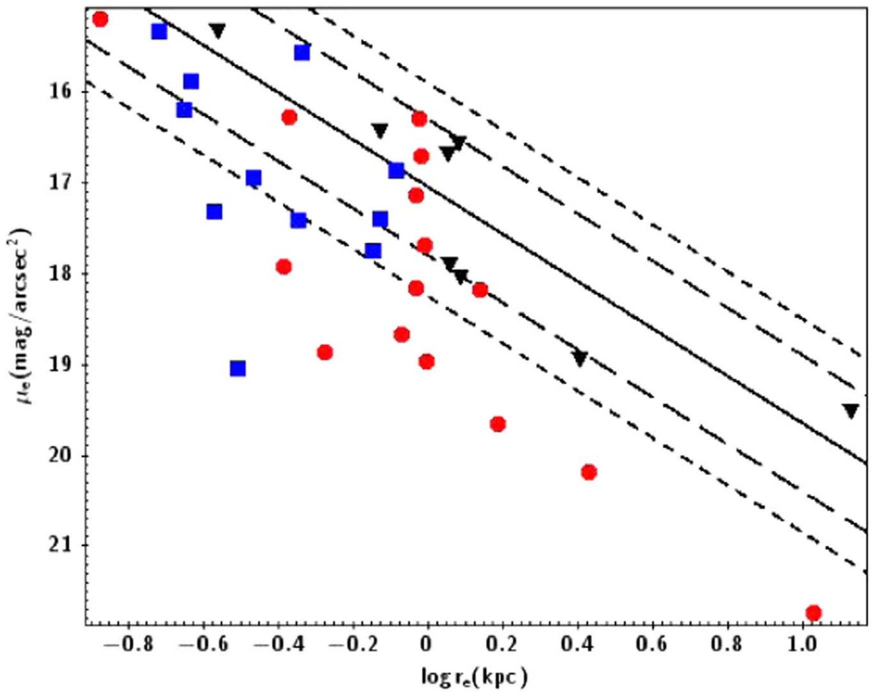

Figure 2. The Kormendy diagram for our sample. The blue filled and open squares represent the classical and pseudo bulges of SB0 galaxies respectively, red filled and open circles correspond to the classical and pseudo bulges of S0 galaxies respectively and black triangles are E/S0 galaxies. The solid line is the linear fit of E/S0 and the upper and lower dashed and dotted lines are the $\pm 3\sigma$ and $\pm 4\sigma$ lines, respectively.

Low mass classical bulges can assemble cool stellar disks rapidly to grow strong bars within a few rotation timescales (Saha 2015). In time, the bar-driven secular processes can transform the initial classical bulge into a flattened rotating stellar system whose central part grows a bar-like component rotating in sync with the disk bar.

7. Discussion and Conclusions

This work aims to study the bulge and bar properties of non-dwarf SB0 galaxies in the central region of the Coma Cluster using the HST/ACS Coma Cluster Treasury Survey. We have identified and characterized bar features using GALFIT, by fitting the bulge, disk and bar components for our sample of SB0 galaxies. We found that the average mass of bulges in barred SB0 galaxies is 1.48×10^{10} $M_{\odot}$ while that for non-barred S0 galaxies is 4.3×10^{10} $M_{\odot}$. This agrees with results from N-body simulations that show that massive bulges make the disk kinematically hot and prevent the formation of bars in galaxies (Athanassoula et al. 2005; Kataria & Das 2018; Cavanagh & Bekki 2020). Bulge mass and bulge concentration also play important roles in the formation of bars in disk galaxies (Kataria & Das 2018). From Figures 3 and 4, we observe that SB0 galaxies manifest smaller bulge concentrations, lower mass and smaller B/T values compared to S0 galaxies.

We classified the bulges based on Sérsic index and the Kormendy relation (Kormendy 1977) as classical and pseudo bulges. Classical bulges are thought to form through the merging of smaller galaxies or through the dissipative collapse of gas in the early universe. They have properties similar to those of elliptical galaxies, such as old populations of stars, little ongoing star formation, and little or no spiral structure.

Pseudo bulges, on the other hand, form through secular processes, such as the slow and steady transfer of material from the disk to the central regions through processes such as bar-driven inflow. They have properties more similar to those of disk galaxies, such as younger populations of stars, ongoing star formation and more prominent spiral structure.

For our sample of barred galaxies, using Sérsic index we found 64% have classical and 36% pseudo bulges. Applying the Kormendy relation, we ascertained that 82% have classical bulges and 18% have pseudo bulges. Cavanagh & Bekki (2020) suggest that strong bars can form in minor mergers and bulges may facilitate bar formation in the galaxy minor mergers and could be the key to explain the formation of bars in lenticular galaxies. Generally, bars are a common feature in pseudo bulge galaxies. How do bars form in classical bulge galaxies? Using *N*-body simulations, Saha (2015) suggests that low mass classical bulges can cause the cool stellar disk to grow rapidly and host a bar within a few rotation timescales. Later, secular processes can transform the initial classical bulge

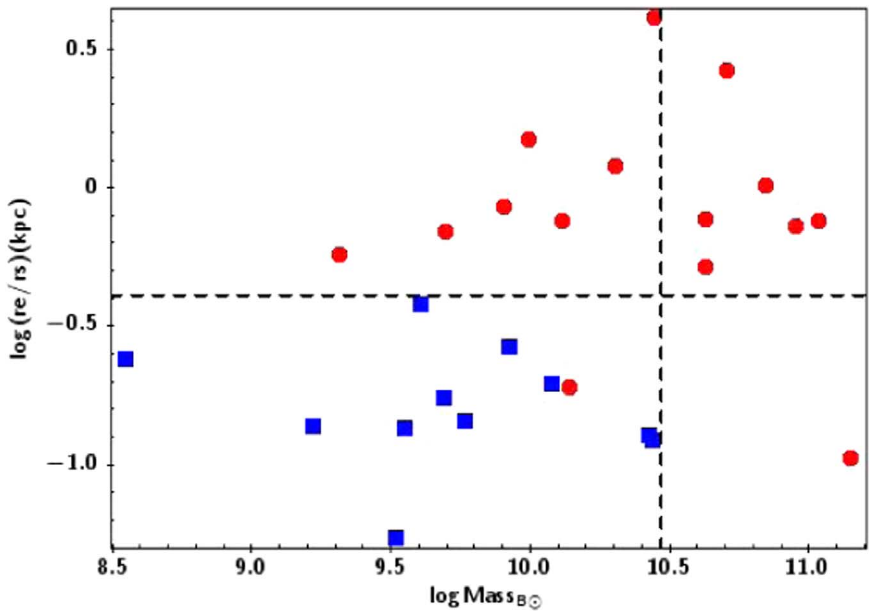

Figure 3. The figure shows a plot of $\log M_{\rm bulge}$ and $\log(r_e/r_s)$ and the locations of SB0 galaxies (blue filled squares) and S0 (red filled circles) galaxies described in the text.

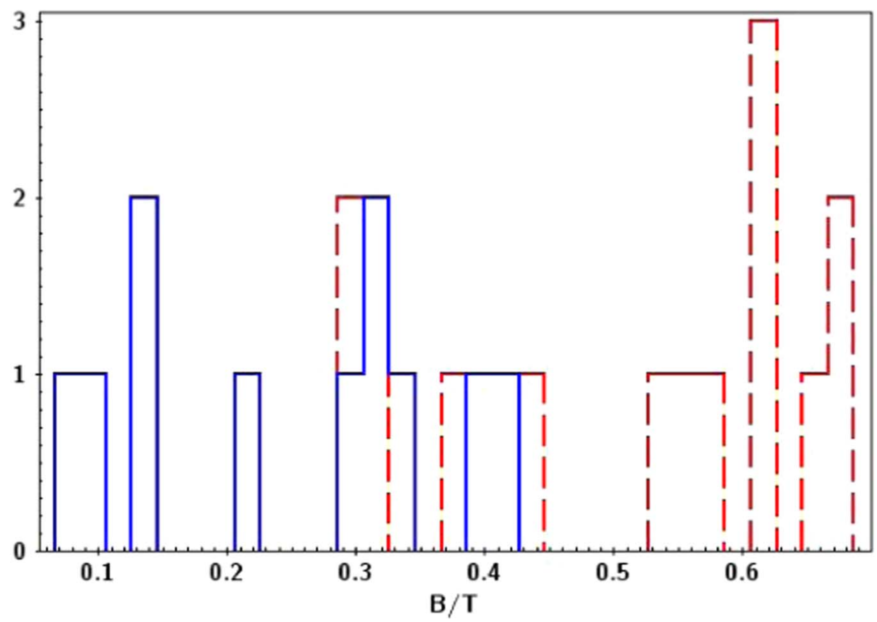

Figure 4. The figure shows the distribution of bulge to total light ratio (B/T). Here blue solid lines represent the SB0 galaxies and red dashed lines correspond to the S0 galaxies.

into a flattened rotating stellar system with a central bar like component rotating in sync with the disk.

In the case of lenticulars in our sample, 11 out of 26 have bars, which also agrees with Aguerri et al. (2009). We observed that of the barred galaxies, 11 are lenticulars and only 2 are spirals. Using the ellipse task in IRAF for field galaxies, Aguerri et al. (2009) found that the bar fraction is distributed with morphological types in the following manner: 29% (lenticular), 55% (early-type spirals) and 54% (late-type spirals). In our sample, of the four spirals, two have bars (50%), which agrees with the above reference. Simulations show that disk instabilities can result in the formation of long-lasting bars throughout a wide range of disk masses. This also implies that bars are strong stellar formations, and that once

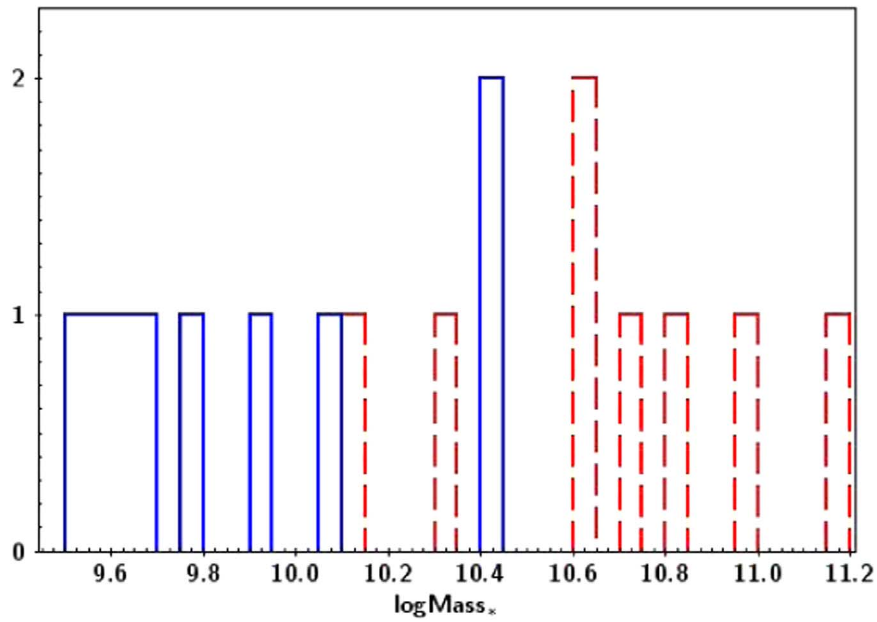

Figure 5. Figure depicts the distribution of logarithm of mass of classical bulges identified by the Kormendy relation. Here blue solid lines represent the classical bulges of SB0 galaxies and red dashed lines correspond to the classical bulges of S0 galaxies.

generated, they are difficult to destroy (Combes & Sanders 1981). Bars in clusters which are dominated by lenticulars are probably formed by minor mergers, while bars in field spiral galaxies have probably formed due to secular evolution.

Larger samples of barred galaxies will help further confirm these results.

Acknowledgments

This study was based on observations made with the NASA/ESA Hubble Space Telescope, obtained from the data archive at the Space Telescope Science Institute (STScI). STScI is operated by the Association of Universities for Research in Astronomy, Inc. under NASA contract NAS 5 − 26555. We thank the reviewer for valuable comments that helped improve our paper.

References

Aguerri, J. A. L., Méndez-Abreu, J., & Corsini, E. M. 2009, A&A, 495, 491
Athanassoula, E. 1999, in ASP Conf. Ser. 160, Astrophysical Discs - an EC Summer School, ed. J. A. Sellwood & J. Goodman (San Francisco, CA: ASP), 351
Athanassoula, E., Lambert, J. C., & Dehnen, W. 2005, MNRAS, 363, 496
Barway, S., Wadadekar, Y., & Kembhavi, A. K. 2011, MNRAS, 410, L18
Bertin, E., & Arnouts, S. 1996, A&AS, 117, 393
Capaccioli, M. 1989, in World of Galaxies (Le Monde des Galaxies), ed. J. Corwin, G. Harold, & L. Bottinelli, 208
Carollo, C. M., Stiavelli, M., & Mack, J. 1998, AJ, 116, 68
Carter, D., Goudfrooij, P., Mobasher, B., et al. 2008, ApJS, 176, 424
Cavanagh, M. K., & Bekki, K. 2020, A&A, 641, A77
Combes, F., & Sanders, R. H. 1981, A&A, 96, 164
Deng, X.-F., He, J.-Z., Chen, Y.-Q., & Jiang, P. 2009, APh, 31, 255
Elmegreen, B. G., Elmegreen, D. M., & Hirst, A. C. 2004, ApJ, 612, 191
Elmegreen, D. M., Elmegreen, B. G., & Bellin, A. D. 1990, ApJ, 364, 415
Fasano, G., Poggianti, B. M., Couch, W. J., et al. 2000, ApJ, 542, 673
Fisher, D. B., & Drory, N. 2008, AJ, 136, 773
Freeman, K. C. 1970, ApJ, 160, 811
Gadotti, D. A. 2008, MNRAS, 384, 420
Gadotti, D. A. 2009, MNRAS, 393, 1531
Gerin, M., Combes, F., & Athanassoula, E. 1990, A&A, 230, 37
Hammer, D., Verdoes Kleijn, G., Hoyos, C., et al. 2010, ApJS, 191, 143
Helsdon, S. F., & Ponman, T. J. 2003, MNRAS, 339, L29
Hopkins, P. F., Croton, D., Bundy, K., et al. 2010, ApJ, 724, 915
Hubble, E., & Humason, M. L. 1931, ApJ, 74, 43
Into, T., & Portinari, L. 2013, MNRAS, 430, 2715
Jogee, S., Barazza, F. D., Rix, H.-W., et al. 2004, ApJL, 615, L105
Kalnajs, A. J. 1972, ApJ, 175, 63
Kataria, S. K., & Das, M. 2018, MNRAS, 475, 1653
Kormendy, J. 1977, ApJ, 218, 333
Kormendy, J. 2013, in Secular Evolution in Disk Galaxies, ed. J. Falcón-Barroso & J. H. Knapen (Cambridge: Cambridge Univ. Press), 1
Kormendy, J., & Kennicutt, R. C. J. 2004, ARA&A, 42, 603
Krist, J. E., Hook, R. N., & Stoehr, F. 2011, Proc. SPIE, 8127, 81270J
Lansbury, G. B., Lucey, J. R., & Smith, R. J. 2014, MNRAS, 439, 1749
Marinova, I., Jogee, S., Bacon, D., et al. 2007, AAS Meeting Abstracts, 211, 97.12
Marinova, I., Jogee, S., Weinzirl, T., et al. 2012, ApJ, 746, 136
Mayer, L., & Wadsley, J. 2004, MNRAS, 347, 277
Méndez-Abreu, J., Sánchez-Janssen, R., & Aguerri, J. A. L. 2010, ApJL, 711, L61
Nair, P. B., & Abraham, R. G. 2010, ApJL, 714, L260
Peirani, S., Hammer, F., Flores, H., Yang, Y., & Athanassoula, E. 2009, A&A, 496, 51
Peng, C. Y., Ho, L. C., Impey, C. D., & Rix, H.-W. 2002, AJ, 124, 266
Poloji, N., Hasan, P., & Hasan, S. 2022a, NewAs, 101963
Poloji, N., Hasan, P., & Hasan, S. N. 2022b, MNRAS, 510, 4463
Price, J., Phillipps, S., Huxor, A., et al. 2009, MNRAS, 397, 1816
Saha, K. 2015, ApJL, 806, L29
Sersic, J. L. 1968, Atlas de Galaxias Australes (Cordoba: Observatorio Astronomico)
Skibba, R. A., Masters, K. L., Nichol, R. C., et al. 2012, MNRAS, 423, 1485
Toomre, A., & Toomre, J. 1972, ApJ, 178, 623
Vaghmare, K., Barway, S., & Kembhavi, A. 2013, ApJL, 767, L33
Weinzirl, T., Jogee, S., Neistein, E., et al. 2014, MNRAS, 441, 3083